Metallomics

PAPER

View Article Online
View Journal | View Issue

Cite this: *Metallomics*, 2020, **12**, 1220

Both metal-chelating and free radical-scavenging synthetic pentapeptides as efficient inhibitors of reactive oxygen species generation†

Gizella Csire,[ab] Laetitia Canabady-Rochelle,[c] Marie-Christine Averlant-Petit,[a] Katalin Selmeczi *[b] and Loic Stefan *[a]

Received 16th April 2020,
Accepted 28th May 2020

DOI: 10.1039/d0mt00103a

rsc.li/metallomics

Reactive oxygen species (ROS) are major sources of oxidative stress playing prominent roles in the development of several pathologies including cardiovascular and neurodegenerative diseases or cancers. The presence of transition biometal ions, specifically copper and iron, induces ROS formation by catalyzing the reduction of molecular oxygen to superoxide anion ($O_2^{\bullet -}$), hydrogen peroxide (H_2O_2) and hydroxyl ($HO^{\bullet}$) radical. To limit ROS production and their detrimental effects, we report on the synthesis, physicochemical studies and antioxidant assays of an innovative series of synthetic pentapeptides exhibiting a dual direct/indirect mode of action, both as iron(III)-chelators and as radical scavengers. These combined effects lead to a drastic reduction of *in vitro* reactive oxygen species production up to 95% for the more reactive hydroxyl radical.

Significance to metallomics

We report herein on a new series of peptides exhibiting iron(III)-chelation abilities from acidic to neutral pH corresponding to conditions in which redox-active iron(III) is found *in vivo*, such as in both the gastrointestinal tract and the lysosomal iron labile pool, and in the blood plasma, respectively. Thanks to their chelating properties and their inherent design, this series of peptides act as effective antioxidants based on a dual indirect (*i.e.*, inhibition of the metal redox activity) and direct (*i.e.*, hydroxyl radical scavenging) mode of action, drastically limiting the production of reactive oxygen species up to −99% for the hydroxyl radical.

Introduction

Metal ions are naturally occurring in living organisms and play pivotal roles in a wide variety of physiological processes including photosynthesis, respiration, metabolism, transmission of nervous influx or protection against pathogenic agents.[1] Among the transition metal ions having *in vivo* roles, copper and iron are associated with several biological processes and the misregulation of their concentration, homeostasis or metabolism are at the origin of pathologies (*e.g.*, Wilson's and Menkes diseases, anaemia, cancers).[2,3] In particular, iron and copper involve the formation of reactive oxygen species (ROS) through the catalytic reduction of molecular oxygen (O_2) to hydrogen peroxide (H_2O_2), superoxide anion ($O_2^{\bullet -}$) and hydroxyl ($HO^{\bullet}$, *via* the Fenton reaction) radicals (Fig. 1a).[4,5] Thanks to a precisely controlled concentration in healthy cells, ROS contribute to complex signalling pathways including metabolism, immune system regulation and proliferation.[6,7] However, under endogenous and exogenous stresses (*e.g.*, pollution, UV-irradiation, tobacco, diet) this homeostasis is dysregulated, and the subsequent overproduction of ROS induces deleterious effects to cells. This so-called oxidative stress has been reported as a source of several pathologies in humans, including respiratory, neurodegenerative, cardiovascular and digestive diseases, and even cancers.[8,9] To prevent or forestall oxidative stress and its damaging effects, the intake of exogenous antioxidant supplementation has proved its effectiveness on ROS regulation.[10] Among the most representative antioxidants, a large majority are natural compounds,[10,11] including ascorbic acid, carotenoids, phenolic derivatives and, more recently, peptides. Bioactive peptides have been attracting growing interests in pharmaceutical, therapeutical and nutraceutical industries and researches thanks to their

[a] *Université de Lorraine, CNRS, LCPM, F-54000 Nancy, France. E-mail: loic.stefan@univ-lorraine.fr*
[b] *Université de Lorraine, CNRS, L2CM, F-54000 Nancy, France. E-mail: katalin.selmeczi@univ-lorraine.fr*
[c] *Université de Lorraine, CNRS, LRGP, F-54000 Nancy, France*

† Electronic supplementary information (ESI) available. See DOI: 10.1039/d0mt00103a

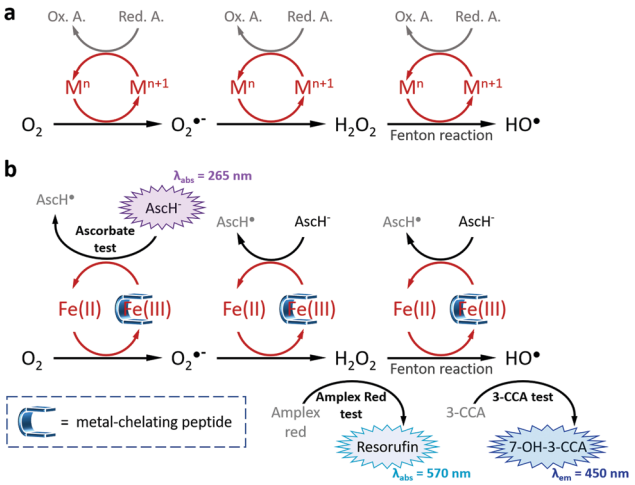

Fig. 1 (a) Schematic representation of transition metal-catalysed ROS formations (M = Fe, Cu; Red. A. = Reducing Agent, Ox. A. = Oxidized Agent) and (b) of the strategy used in this work to inhibit ROS formations *via*, *inter alia*, the chelation of Fe(III). The three tests allowing the measure of the antioxidant properties of the metal-chelating peptides are depicted with their corresponding absorbance or emission wavelengths.

inherent advantages in terms of diversity, modularity, selectivity, efficiency, safety and tolerability.[12,13] Thus, several antioxidant peptides have been reported, mainly identified *a posteriori via* LC/MS/MS analyses from hydrolysates of natural resources[14,15] (*e.g.*, milk, vegetables, cereals,[16,17] algae, animals[18]) exhibiting antioxidant activities. However, this usual approach remains challenging and suffers from several drawbacks:[14,19] time-consuming, expensive, hazardous and uncertain in terms of quantity and recovery, drastically limiting the discovery of effective antioxidant peptides. To tackle these issues, we assume that a more rational strategy is required; thus, we report herein on the design, synthesis, physicochemical studies and antioxidant assays of a new series of pentapeptides exhibiting drastic inhibition of ROS production thanks to a dual direct/indirect mode of action, *i.e.*, both Fe(III)-chelating and radical scavenging properties.

Results and discussion

Design and synthesis of antioxidant peptides

The indirect mode of action is based on metal chelation, an approach that has demonstrated its effectiveness on reduction of ROS production and on ROS-mediated pathologies.[10,20–22] Among the most studied aforementioned metal-chelating antioxidants, we can mention polyphenols[23] including flavonoids[24,25] (*e.g.*, quercetin,[26] epigallocatechin-3-gallate[20,27]), resveratrol[28] or curcumin,[29] capsaicin,[30] quinolines (*e.g.*, clioquinol,[21] 8-hydroxyquinoline derivatives[20,31]), and the siderophores deferiprone[32] and deferoxamine (this latter will be further discussed below). While metal-chelating peptides have been widely studied in the last decades for their copper-binding properties,[33,34] Fe(III) has hardly been considered, with only few examples of peptides[35] and peptide derivatives functionalized with well-known

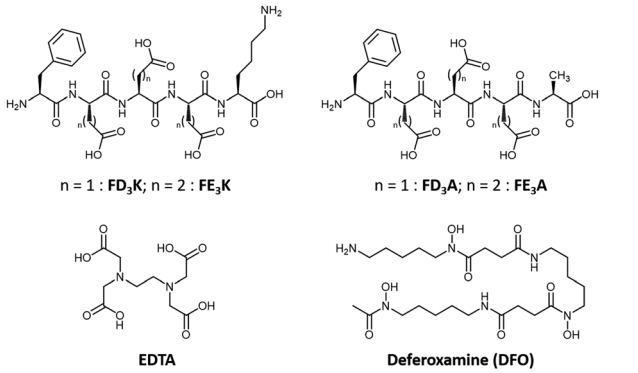

Fig. 2 Chemical structures of the four peptides studied (top), the negative control EDTA (bottom left) and the positive control DFO (bottom right).

iron-chelating chemical moieties (*e.g.*, EDTA, hydroxamate).[36–38] Besides meeting this challenge, we selected Fe(III) as a target metal ion instead of Fe(II), because of its: 1/unusual +III oxidation state (only shared with Al^{3+}, Cr^{3+} and Co^{3+} ions in a biological context),[39] 2/stability in aerobic conditions, 3/specific coordination properties (*i.e.*, while Cu(I), Cu(II) and Fe(II) are classified as soft acid and borderline, respectively, Fe(III) is a hard acid).[40] Based on the Pearson's HSAB theory, we developed a series of four peptides comprised of acidic amino acid (*i.e.*, aspartates (D), or glutamates (E)) triads acting as hard Lewis bases (Fig. 2). In C-terminal position, two amino acids were considered: alanine (A, uncharged, hydrophobic) and lysine (K, bringing an additional positive charge to improve water-solubility). The direct antioxidant mode of action, *i.e.*, radical scavenging, originates from the phenylalanine (F) introduced at the N-terminal position. Already reported as a biomarker of oxidative stress,[41,42] the sensitivity of phenylalanine to ROS is harnessed herein to entrap the hydroxyl radicals produced at the contiguous catalytic metal centre during the Fenton reaction. Thus, peptides have been synthesized by solid-phase peptide synthesis using a Fmoc/^{t}Bu strategy, purified by RP-HPLC and fully characterized by HPLC, ESI-HRMS and ^{1}H, ^{13}C and 2D NMR (see ESI† for details).

Evaluation of the iron(III)-chelation properties

Potentiometric studies were carried out on the synthesised compounds, in the presence and absence of Fe(III). Such titrations were essential to both access the species distributions as a function of pH and to obtain characteristic dissociation constants of the peptides and stability constants of iron(III) complexes. The deprotonation constants of the ligands are listed in Table 1. These ligands have five or six protonable groups: four carboxyl groups and one or two amino groups. Only the deprotonations of the three side chain carboxyl functions were measurable in the studied pH range (pH 2–11), since the terminal COOH probably has a pK < 2. The COOH deprotonation processes are overlapping, thus their pK values cannot be assigned to the distinct donor groups. The basicity of the terminal amino groups corresponds well to the values measured for other ligands.[43,44] Potentiometric titration, CD and ^{1}H/^{13}C NMR measurements were carried out in order to obtain

Table 1 Overall protonation constants ($\log\beta$ H_iL) and deprotonation constants (pK) of the four studied peptides (T = 298 K, I = 0.1 M $NaNO_3$ (standard deviations are in parentheses))

$\log\beta$	FD_3K	FE_3K	FD_3A	FE_3A
HL	10.98 (3)	10.82 (3)	7.77 (1)	7.66 (2)
H_2L	18.62 (3)	18.32 (3)	12.55 (3)	12.73 (6)
H_3L	23.25 (4)	23.18 (5)	16.47 (5)	16.92 (7)
H_4L	26.99 (5)	27.27 (5)	20.11 (5)	20.97 (9)
H_5L	30.70 (5)	31.10 (6)	—	—
pK				
COOH	3.71 (5)	3.83 (6)	3.64 (5)	4.05 (9)
COOH	3.74 (5)	4.09 (5)	3.92 (5)	4.19 (7)
COOH	4.63 (4)	4.86 (5)	4.78 (3)	5.07 (6)
NH_3^+ (N_{term})	7.64 (3)	7.50 (3)	7.77 (1)	7.66 (2)
ε-NH_3^+ (Lys)	10.98 (3)	10.82 (3)	—	—

information on the Fe(III)-pentapeptide complexes. Stability constants and pK values can be found in Table 2. In the case of FE_3A and FD_3A precipitation occurred at a low pH (<5), therefore the constants have a greater error.

The chelation of Fe(III) by three of the four peptides (except for FE_3A) started at pH 2 and only monocomplexes were formed. For FE_3A the complexation started at higher pH, near pH 3. The species distribution curves of the Fe(III):ligand systems in 1:1 and 1:2 ratio are depicted in Fig. 3 and allow to observe significant differences between the peptides in terms of chelation ability: while FD_3K is effective up to pH 7.6, FE_3K releases iron beyond pH 6, FD_3A and FE_3A do the same from pH 5. Analysis by ^{1}H NMR measurements of the solution after complete precipitation showed that only the free peptides were kept in solution. Based on the spectroscopic information discussed later, the metal ion is coordinated by 3 COO^- groups in FeH_3L species (lysine-containing peptides) or in FeH_2L (FD_3A) (Table 2), and the next deprotonation step can be attributed to the fourth COOH deprotonation and its coordination to Fe(III). This statement is also supported by the downshifted values of the carbonyl deprotonation constants. Indeed, for the sake of example, $pK_{FD3K}(H_3L/H_2L)$ = 4.63 corresponding to the deprotonation of the fourth carboxylic acid in the free FD_3K peptide is downshifted to $pK(FeH_3L/FeH_2L)$ = 3.36 in the presence of one equivalent of Fe(III), indicating a metal chelation *via* the carboxylate groups (*i.e.*, aspartate or glutamate side chains and C-terminal carboxylate). To explain the further steps above pH 3, consecutive deprotonations of coordinated water molecules is suggested to form firstly {$4COO^-$, OH^-} coordination environment in FeHL species in the case of peptides containing lysine, and in FeL species in the case of alanine-containing ligands (Table 2). The deprotonation of the second coordinated water gave a {$4COO^-$, $2OH^-$} coordination sphere around the iron(III) ion with the ligands FD_3K and FE_3K, but led to the iron precipitation with FD_3A and FE_3A. Interestingly, the primary amines from both the lysine and the N-terminal are not involved in the chelation, evidenced by similar dissociation constant both in the presence or in the absence of Fe(III) (pK = 7.64 and 7.54 for FD_3K, respectively). Moreover, iron precipitation started with deprotonation of NH_3^+ (N-term) in the case of lysine-containing FD_3K peptide.

As a standard for measuring and comparing the effectiveness of potential chelating agents for a metal ion, the concentration of the uncomplexed aqueous ion in solution can be calculated under specific conditions. Noted as pM = $-\log[M_{free}]$, this value provides more relevant information than $\log K_{ML}$ since it takes into account the ligand basicity, the pH, the ligand:metal ratio and the metal ion hydrolysis. The pM values are calculated for FD_3K, FE_3K, EDTA and DFO at 100 μM concentration with 1:1 ligand-to-Fe(III) ratio at pH 6.0 and 7.4, and tabulated in Table 3. The higher the pM value, the greater the affinity of the ligand to the iron(III) under these specific conditions used for the measurement of antioxidant activity (*vide infra*). The data show that the pentapeptides are not as strong complexing agents than EDTA[46] or DFO[45] (Fig. 2) because they leave more free Fe(III) in solution regardless of the pH. Precipitation as iron(III) hydroxide is produced if the pM value is lower than the limit set by the K_{sp} of $Fe(OH)_3$.

Extrapolating these potentiometric data to a *in vivo* context, we can first assume that such pentapeptides will be able to chelate iron(III) ions in acidic and slightly acidic biological media. For instance, they could chelate dietary non-heme iron in the gastrointestinal tract (pH from 2 to 8), mainly in the duodenum and the jejunum where iron is present in its ferric

Table 2 Stability constants ($\log\beta$) and derived data (pK) for Fe(III) complexes of the four studied peptides (T = 298 K, I = 0.1 M $NaNO_3$ (standard deviations are in parentheses))

	FD_3K	FE_3K	Peptide protonation state (in bold coordinated to Fe(III))	Global charge	FD_3A	FE_3A	Peptide protonation state (in bold coordinated to Fe(III))
	$\log\beta$				$\log\beta$		
FeH_3L	29.61 (2)	30.02 (3)	**3 COO^-**, ε-NH_3^+ (Lys), NH_3^+ (N_{term})	+2	—	—	
FeH_2L	26.25 (3)	26.25 (5)	**4 COO^-**, ε-NH_3^+ (Lys), NH_3^+ (N_{term})	+1	17.61 (13)	—	**3 COO^-**, NH_3^+ (N_{term})
FeHL	22.17 (3)	21.87 (5)	**4 COO^-**, **OH^-**, ε-NH_3^+ (Lys), NH_3^+ (N_{term})	0	14.53 (7)	13.82 (11)	**4 COO^-**, NH_3^+ (N_{term})
FeL	17.08 (3)	16.88 (4)	**4 COO^-**, **2 OH^-**, ε-NH_3^+ (Lys), NH_3^+ (N_{term})	−1	10.19 (11)	9.23 (19)	**4 COO^-**, **OH^-**, NH_3^+ (N_{term})
$FeH_{-1}L$	9.54 (5)	—	**4 COO^-**, **2 OH^-**, ε-NH_3^+ (Lys), NH_2 (N_{term})	−2	4.72 (13)	4.23 (18)	**4 COO^-**, **2 OH^-**, NH_3^+ (N_{term})

pK	FD_3K	FE_3K	Deprotonated group	FD_3A	FE_3A	Deprotonated group
pK (FeH_3L/FeH_2L)	3.36	3.77	COOH	—	—	
pK ($FeH_2L/FeHL$)	4.08	4.38	H_2O	3.08	—	COOH
pK (FeHL/FeL)	5.09	4.99	H_2O	4.34	4.59	H_2O
pK ($FeL/FeH_{-1}L$)	7.54	—	NH_3^+ (N_{term})	5.47	5.00	H_2O

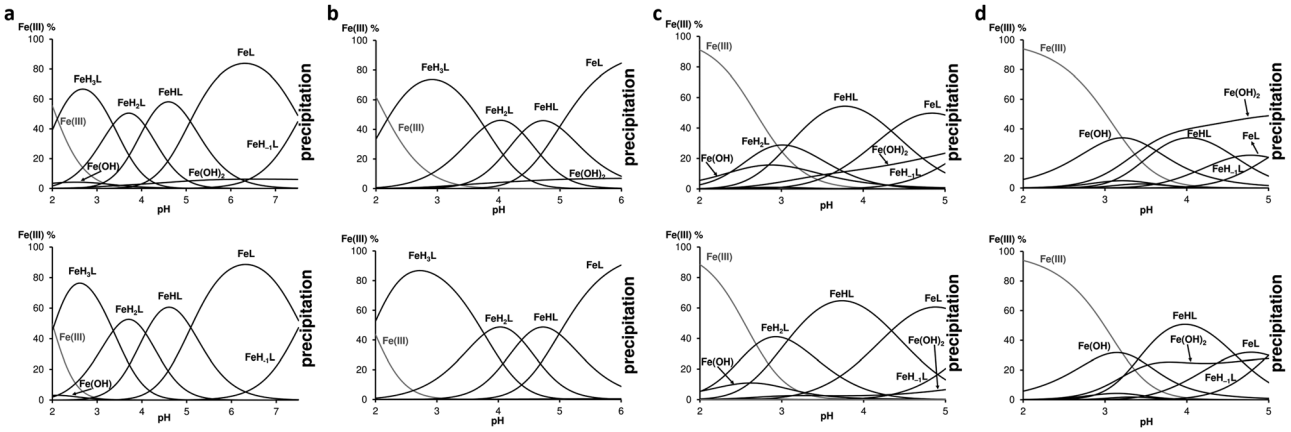

Fig. 3 Speciation diagrams of (a) Fe(III)-FD_3K 1 : 1 (top) and 1 : 2 (bottom) systems, (b) Fe(III)-FE_3K 1 : 1 (top) and 1 : 2 (bottom) systems, (c) Fe(III)-FD_3A 1 : 1 (top) and 1 : 2 (bottom) systems and (d) Fe(III)-FE_3A 1 : 1 (top) and 1 : 2 (bottom) systems. For all the experiments $[peptide]_{tot}$ = 2 mM, T = 298 K, I = 0.1 M $NaNO_3$.

Table 3 Free iron(III) concentrations at equilibrium (M) and pM (= $-\log[M_{free}]$) values calculated from ligand protonation and complex stability constants for 100 μM ligands and Fe(III) at pH 6.0 and 7.4 at T = 298 K, I = 0.1 M $NaNO_3$

	Free iron(III) concentration (M)		pM value	
	pH 6	pH 7.4	pH 6	pH 7.4
DFO[45]	1.22×10^{-16}	6.12×10^{-20}	15.91	19.21
EDTA[46]	5.84×10^{-16}	3.00×10^{-18}	15.23	17.52
FD_3K	9.67×10^{-11}	1.52×10^{-13}	10.01	12.82
FE_3K	9.06×10^{-11}	—	10.04	—
Fe(III) alone[47]	3.16×10^{-15}	2.00×10^{-19}	14.50	18.70

form, and subsequently influence iron absorption.[48,49] The pentapeptides could also interact with iron(III) ions from the labile iron pool, a pool of chelatable and redox-active iron playing pivotal roles in the formation of ROS, and in particular from the lysosomal labile pool in which iron is in its free iron(III) form and in an acidic (pH ≈ 4.5–5) environment.[50,51] In parallel, potentiometric measurements also revealed that only one peptide, namely FD_3K, forms a stable complex at pH 7.4, corresponding to the pH of the blood plasma (also referred as "physiological pH"). In the plasma of healthy individuals iron is sequestrated by circulating transferrin forming highly stable complexes ($\log K \approx 23$)[52] which drastically limit the possibilities of chelation by FD_3K. However, in the case of long-term transfusions for patients with anemia caused by several genetic disorders (*e.g.*, thalassemia, sickle cell disease), a systemic iron overload is observed, surpassing the total iron binding capacity (*i.e.*, saturating transferrin).[53,54] In these conditions, labile plasma iron is circulating and a chelator, such as our pentapeptide FD_3K could entrap the residual labile iron and limit its detrimental effects.

To gain further insights into the chelation behaviors of the four pentapeptides, circular dichroism and paramagnetic ^1H and ^{13}C NMR measurements were carried out. The experiments endorsed the potentiometric results and confirmed the chelation of the peptides through their carboxylate functions. The CD spectra were recorded at different pH with the ligands alone and also in the presence of iron(III) ion in ratio M : L = 1 : 1 (Fig. 4a and Fig. S1, S2, ESI†). The free FD_3K ligand had a positive or a negative band with variable intensity below 250 nm in function of pH (Fig. S1, ESI†). Starting from acidic pH, with subsequent deprotonation of the side chain carboxyl groups, the negative CD band changed sign indicating conformational changes in the structure. When all the carboxyl groups are deprotonated, the CD band changed sign again following the deprotonation of terminal amino group (Fig. S1, right, ESI†). When 1 eq. iron(III) was added to the solution, the CD spectrum was already different at pH 2, the Cotton effect appeared above 250 nm (Fig. 4a and Fig. S2, left, ESI†), especially the appearance of a charge transfer band at 290 nm or at 330 nm due to the interaction between iron(III) and the carboxylate groups from aspartic acid containing peptides or glutamic acid containing ligands, respectively (Fig. 4a).[55] With increasing pH, the CD spectra indicated considerable changes compared to the free peptide, the intensity of the charge transfer band diminished with the deprotonation of coordinated water molecules (Fig. S2, right, ESI†). In order to confirm the iron(III) ion coordination environment, paramagnetic NMR experiments were performed in the presence of a high excess of FD_3K and FE_3K peptides. Indeed, the presence of unpaired electron(s) of metal ion gives rise to large shifts and/or broadening effects on the NMR resonances of nuclei in close proximity. In our case, in the presence of weak donor atoms like carboxylates, the iron(III) ion is in high spin state (S = 5/2), which has a relatively long electron relaxation time (τ_s of the order of 10^{-9}–10^{-11} s) because the electron relaxation mechanisms are relatively inefficient.[56] The spectral resolution is also affected by the exchange rate between the free ligand and the ligand bound to the paramagnetic metal ion. Thus, due to the labile character of iron(III), at low M : L ratio (1 : 6) the ^1H NMR signals were too broad to be attributable (Fig. S5 and S6, ESI†). The line broadening effects are less significant for ^{13}C nucleus, which makes NMR detection more advantageous for the identification of residue near the paramagnetic centre.[57] Thus, on the ^{13}C spectra (Fig. 4b and c) the most affected signals were assigned to the carbon atoms of four carboxylate groups (C10, C13, C15 and C17 for FD_3K; C10, C14, C17 and C20 for FE_3K). Signals of α-carbon relative to

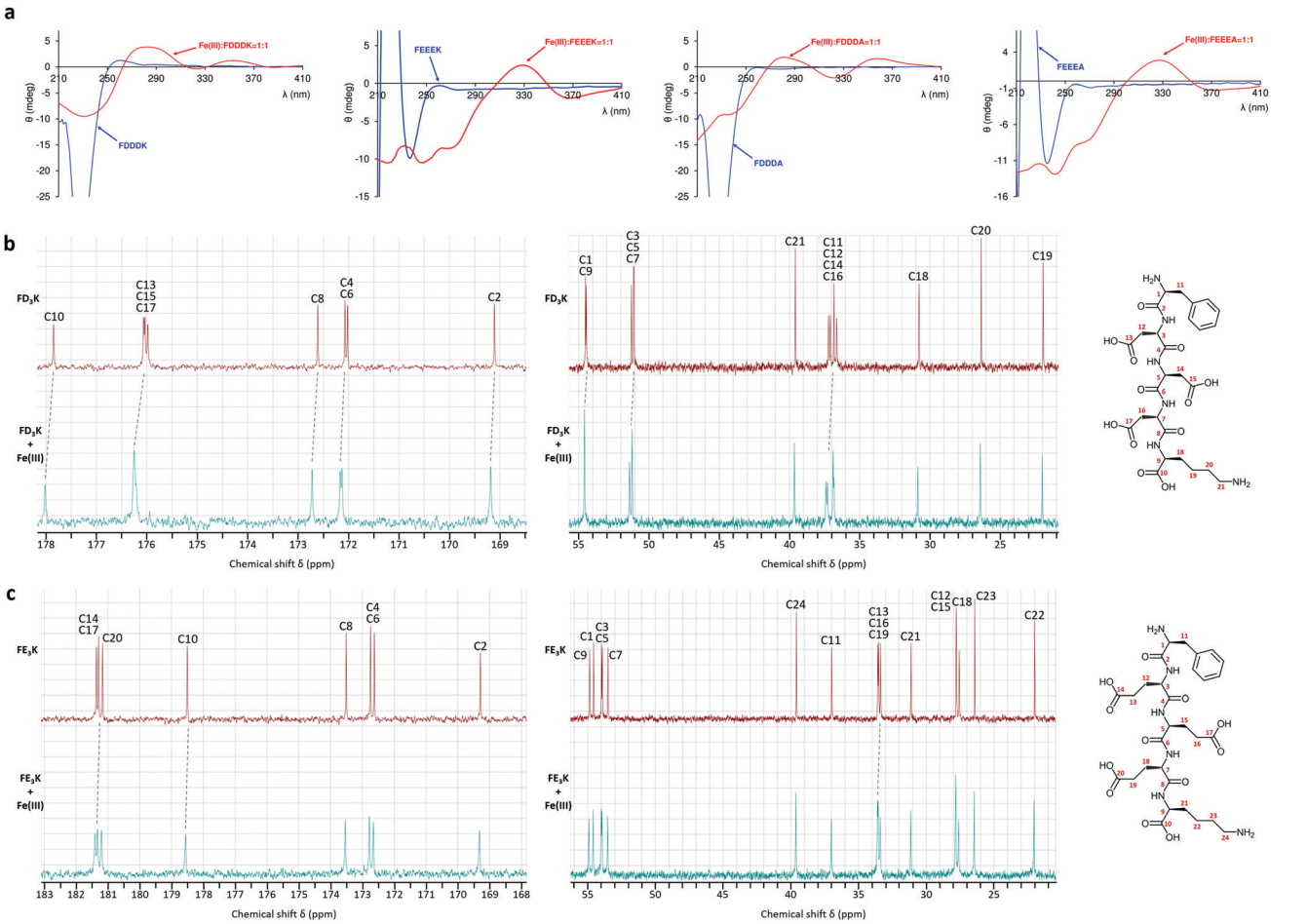

Fig. 4 (a) Circular dichroism spectra of the free ligand (blue lines) and iron(III) complexes (red lines) in ratio M : L = 1 : 1 at pH 3. ^{13}C NMR spectra of (b) FD_3K and (c) FE_3K alone (in red) and in the presence of Fe(III) (in cyan) in ratio M : L = 1 : 6 and 1 : 5, respectively.

carboxylate seemed to be also affected (C9, C12, C14, C16 for FD_3K; C13, C16, C19 for FE_3K). No carbon atom signals from the N-terminal phenylalanine or from the side chain of lysine were broadened confirming that no NH_2 group are present in the iron(III) coordination environment.

Antioxidant properties

To assess the antioxidant properties of the two more efficient Fe(III) chelators FD_3K and FE_3K, a global approach considering several aspects of the antioxidant process, namely the metal redox activity and the formation of different types of ROS (Fig. 1b), have been used. For comparison purpose, we selected two reference iron(III)-chelating ligands ensuring iron solubility in a wide range of pH and offering opposite antioxidant properties. EDTA (for ethylenediaminetetraacetic acid, Fig. 2) has been chosen as a negative control based on its weak antioxidant capabilities well-documented since the 1980's,[58–61] while deferoxamine (also termed DFO, Fig. 2), an approved drug used for half a century to treat iron overload and reported as an efficient *in vitro*[59–61] and *in vivo* antioxidant,[62] has been considered as our positive control. Thus, antioxidant experiments were firstly carried out at pH 6.0 to ensure the stability of the two Fe(III)-pentapeptide complexes (*vide supra*). To evaluate the reducibility of Fe(III) to Fe(II), we performed the ascorbate test[63,64] in which the consumption of ascorbate ($AscH^-$, playing the role of reducing agent, Fig. 1), is monitored as a function of time by UV-vis spectroscopy (λ_{abs} = 265 nm). While no variation was observed in the absence of metal ion after 10 min (Table S1 and Fig. S7, ESI†), consumption of $AscH^-$ occurred in the presence of Fe(III) with a maximum observed for the negative control EDTA with 32 μM $AscH^-$ consumed (Fig. 5a). The use of FD_3K or FE_3K induces a decrease of this value to 19.5 μM and 18.3 μM, corresponding to a reduction of 39% and 43%, respectively, compared to EDTA. These data highlight the ability of the two pentapeptides to inhibit the redox activity of Fe(III), even if less efficient than the positive control DFO (6.6 μM $AscH^-$ consumed, 79% reduction relative to EDTA). To evaluate the impact of this limited Fe(III) redox activity on the production of ROS, two different assays were considered for two different ROS species (*i.e.*, H_2O_2 and $HO^\bullet$, Fig. 1b). Firstly, the production of H_2O_2 was monitored by UV-vis spectroscopy due to its ability to oxidize Amplex Red to the coloured Resorufin (λ_{abs} = 570 nm) in the presence of horseradish peroxidase (HRP).[65,66] As depicted in Fig. 5b, the presence of FD_3K and FE_3K induces a strong decrease of H_2O_2 formation by 88% and 89%, corresponding to 2.0 μM and 1.8 μM H_2O_2, respectively, compared to the negative

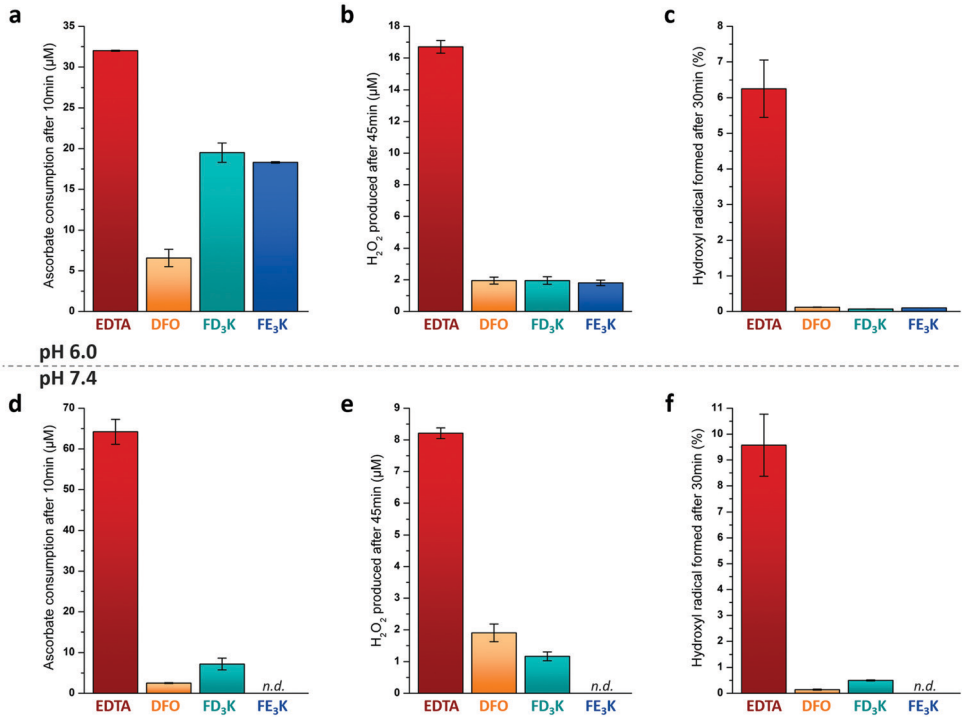

Fig. 5 (a and d) Consumed $AscH^-$ concentrations after 10 min reaction at pH 6.0 (a) or pH 7.4 (d) (50 mM HEPES buffer). $[AscH^-]_0$ = $[Ligand]_0$ = 100 μM and $[Fe(III)]_0$ = 100 μM. (b and e) Produced H_2O_2 concentrations after 45 min reaction at pH 6.0 (b) or pH 7.4 (e) in water. $[AscH^-]_0$ = 200 μM, $[Ligand]_0$ = 50 μM and $[Fe(III)]_0$ = 50 μM. (c and f) Formed $HO^•$ concentrations after 30 min reaction at pH 6.0 (c) or pH 7.4 (f) in water. $[AscH^-]_0$ = 125 μM, $[Ligand]_0$ = 50 μM and $[Fe(III)]_0$ = 50 μM in the case of peptides (FD_3K, FE_3K) and DFO. $[AscH^-]_0$ = 12.5 μM, $[Ligand]_0$ = 5.0 μM and $[Fe(III)]_0$ = 5.0 μM in the case of EDTA. All experiments were carried out at 298 K. *n.d.* for not determined.

control EDTA (16.7 μM H_2O_2 formed). Interestingly, both pentapeptides exhibit similar high efficiencies than the positive control DFO (1.9 μM H_2O_2 produced). Secondly, the formation of the more reactive hydroxyl radical was studied using the 3-CCA (for coumarin-3-carboxylic acid) assay in which 3-CCA reacts with $HO^•$ to generate the fluorescent 7-OH–3-CCA (λ_{ex} = 395 nm, λ_{em} = 450 nm) followed spectrofluorimetrically.[67] Once again, the two peptides strongly inhibit the $HO^•$ production with a decrease of 98% (FD_3K) and 99% (FE_3K), similar to DFO (Fig. 5c). Altogether, these data confirm the high antioxidant efficiency of FD_3K and FE_3K thanks to their inhibition of both Fe(III) redox activity and ROS productions. However, these peptides have only a moderate binding ability as previously discussed by comparing pM values relative to EDTA and DFO (Table 3). Interestingly, EDTA has a very good complexation capacity but is not able to protect iron(III) from reduction. These known properties of the EDTA–Fe(III) complex can have different origins such as its unusual heptacoordinated structure[68] and the N/O-type donor atoms, which are less suitable to hard iron(III) ion than the purely O-donor atoms as in DFO, or in the FD_3K and FE_3K peptides. These observations highlight the importance of both the binding groups and the geometry around the metal ion, which strongly impact the antioxidant properties. Concerning FD_3K and FE_3K peptides, the nature of the acidic amino acid (*i.e.*, aspartate or glutamate) does not significantly affect the global antioxidant properties; however, the Fe(III)–FD_3K complex has a better stability in a broader range of pH (*vide supra*, Fig. 3a and b), offering better opportunities for biomedical applications. Thus, antioxidant studies were carried out on this peptide at physiological pH (≈ pH 7.4). The ascorbate test (Fig. 5d) reveals a strong inhibition of the redox activity when Fe(III) is chelated by FD_3K compared to EDTA with a decrease of 89% of the $AscH^-$ consumption. The reduction of H_2O_2 and $HO^•$ productions by 86% and 95% (Fig. 5e and f), respectively, is also highly significant, close to the DFO efficiency (−76% for H_2O_2, −98% for $HO^•$). Thus, FD_3K has confirmed its antioxidant properties both at pH 6.0 and at physiological pH through its ability to chelate Fe(III), reducing the metal redox activity and, *in fine*, the ROS formation.

Besides this indirect antioxidant mode of action, peptides have also been designed as radical scavengers to entrap the radicals formed at the metal centre (direct antioxidant mode of action), thanks to the phenylalanine moiety grafted at the N-term.[69] To study this effect, a series of mass spectroscopy analyses were performed (Fig. 6a). The MS spectrum of a solution containing Fe(III)/$AscH^-$/FD_3K (Fig. 6a, in red) reveals the presence of the peptide at m/z = 639.259 ($[FD_3K + H]^+$) and of another peak at m/z = 655.250 corresponding to $[FD_3K + H + O]^+$, *i.e.*, a mono-oxidized form of the peptide. To improve the signal and to determine which ROS triggers the oxidation, an H_2O_2 supplementation has been added to the Fe(III)/$AscH^-$/FD_3K mixture (Fig. 6a, in dark cyan) in order to favour the *in situ* formation of $HO^•$. In these conditions, the $[FD_3K + H + O]^+$/$[FD_3K + H]^+$ signal intensity ratio increased, confirming the

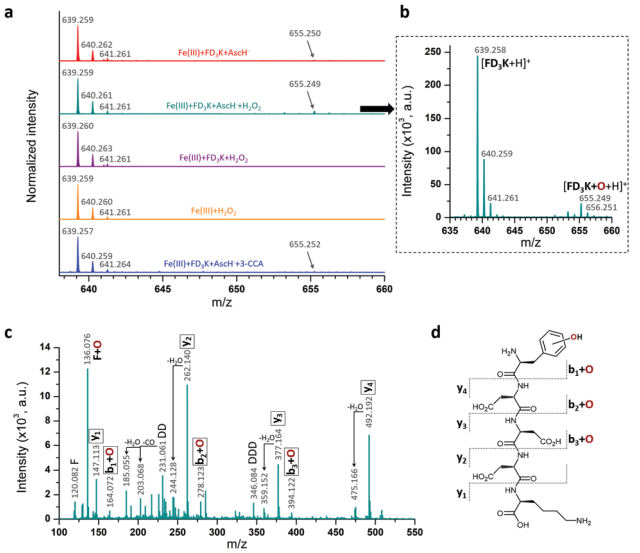

Fig. 6 (a) HRMS spectra of FD_3K oxidation by HO• radical. Red spectrum: [Fe(III)] = [FD_3K] = [$AscH^-$] = 1 mM, dark cyan spectrum: [Fe(III)] = [FD_3K] = [$AscH^-$] = [H_2O_2] = 1 mM (a zoom is provided in b), purple spectrum: [Fe(III)] = [FD_3K] = [H_2O_2] = 1 mM, orange spectrum: [Fe(III)] = [H_2O_2] = 1 mM, blue spectrum: [Fe(III)] = [FD_3K] = [$AscH^-$] = [3-CCA] = 1 mM. (c) HRMS/MS spectrum at m/z = 655.249 and (d) Proposed fragmentation schema of oxidized FD_3K peptide.

involvement of HO• in the oxidation process. The oxidized peptide at m/z = 655.249 has been subsequently analysed by HRMS/MS (Fig. 6c) and the fragmentation confirms the formation of an oxidized phenylalanine, *i.e.*, a hydroxyl-phenylalanine, as previously reported.[41,42] To discard the possibility of an H_2O_2-induced oxidation, two control conditions were analysed: one with a Fe(III)/FD_3K/H_2O_2 mixture (*i.e.*, without the reducing agent $AscH^-$) and one with a FD_3K/H_2O_2 mixture. For both, no detectable peak corresponding to the oxidized peptide has been observed: FD_3K is therefore insensitive to H_2O_2. As a further control experiment, 3-CCA (the reactant used to evaluate the amount of HO• radicals formed, *vide supra*) was added to the Fe(III)/$AscH^-$/FD_3K mixture, and the corresponding HRMS analysis (Fig. 6a, in blue) reveals the presence of the oxidized peptide. Such results highlight that once formed at the metal centre, hydroxyl radicals are both reacting with surrounding molecules (3-CCA in this case) and entrapped by the peptide (*i.e.*, thanks to the hydroxylation of the phenylalanine), confirming the dual mode of action of this latter. Thus, these data highlight the ability of the peptide to act as a HO• radical scavenger, due to the hydroxylation of the phenylalanine moiety.

Conclusion

In summary, we reported on the very first Fe(III) peptide chelators exhibiting antioxidant properties thanks to a dual indirect (*i.e.*, inhibition of the metal redox activity) and direct (*i.e.*, HO• radical scavenging *via* phenylalanine hydroxylation) mode of action. In particular, we highlighted that the FD_3K pentapeptide strongly inhibits both the iron redox activity (up to −89%) and the ROS production (−86% and −95% for H_2O_2 and HO•, respectively) at physiological pH, rivalling with deferoxamine (DFO), a clinically used iron chelator and antioxidant standard.[59,60,62] Contrasting with the fastidious and hazardous methods commonly used,[14–16,18] this work demonstrates the relevance and the efficiency of a more rational approach to discover new antioxidant peptides. We assume that a comprehensive overview of the peptide properties from the physicochemical key parameters (*e.g.*, metal/ligand stoichiometry, chemical groups involved) to the impact on the iron redox activity and on the ROS formation is required to decipher and understand the parameters governing the antioxidant peptide capabilities, paving the way to the development of more efficient compounds.

Materials and methods

Generalities

Reagents, chemicals and solvents were purchased from Sigma-Aldrich, except Fmoc-L-Glu(O^{t}Bu)-OH, Fmoc-L-Asp(O^{t}Bu)-OH, Fmoc-L-Phe-OH and preloaded Wang resins from Iris Biotech, sodium hydroxide from VWR. All reagents and chemicals were used without further purification. Peptides were synthesized on an automated ResPep XL synthesizer from Intavis AG, and subsequently purified by semi-preparative reversed-phase HPLC using a Macherey-Nagel Nucleosil 100-5 C_{18} 250 × 21 mm column on a Waters HPLC system (equipped with a Waters 600 pump, a Waters 600 controller and a Waters 486 tunable absorbance detector). Analytical reversed-phase HPLC were carried out using a Macherey-Nagel Nucleosil 100-5 C_{18} 250 × 4.6 mm column on a Shimadzu Prominence UFLC (equipped with a LC20AB solvent delivery, SPD-M20A diode array detector and a CTO-20AC column oven). NMR spectra (^{1}H, ^{13}C, HMQC, HMBC, COSY) were recorded at 298 K on a Bruker DRX 400 spectrometer on the NMR Platform of the Jean Barriol Institute (Université de Lorraine, Nancy, France). All analysed samples were aqueous solution at known pH, 1,4-dioxane was used as external standard in capillary (^{1}H δ = 3.75 ppm, ^{13}C δ = 67.2 ppm, dissolved in D_2O). For ^{1}H NMR spectra, a WATERGATE pulse sequence was used for water suppression. High resolution ESI-MS analyses were performed on a Bruker Daltonics MicrOTOFQ mass spectrometer provided by the MassLor Platform (Université de Lorraine, Nancy, France). Circular dichroism spectra were recorded on a MOS-450 spectrometer from BioLogic, coupled with a Metrohm 716 titrator combined with a Fisher Bioblock electrode for pH adjustments. For potentiometric measurements, a Dosimat 715 and a pH-meter equipped with a semi-micro combined electrode from Metrohm were used. UV-vis spectra were recorded on a PerkinElmer Lambda1050 spectrophotometer, room temperature fluorescence emission spectra were recorded on a Fluorolog-3 spectrofluorometer from Horiba Scientific.

Peptide synthesis

The four peptides were synthesized at a 400 μmol-scale using a Fmoc/^{t}Bu strategy and double couplings for each amino acid. The experimental conditions for each coupling were:

Fmoc-amino acid (6 equivalents), 2-(1*H*-benzotriazol-1-yl)-1,1,3,3-tetramethyl-uronium tetrafluoroborate (HBTU, 5 equivalents), and 4-methylmorpholine (NMM, 10 equivalents) in dimethylformamide (DMF) and *N*-methyl-2-pyrrolidone (NMP), coupling time = 40 minutes. Fmoc-deprotection steps were carried out using a 20% piperidine solution in DMF (3 × 15 min), and final cleavages were achieved using a trifluoroacetic acid/triisopropylsilane/water (92,5/5/2,5) mixture (2 hours). The crude peptides were precipitated from cold diethylether (−20 °C), centrifuged, washed with cold diethylether, dried under reduced pressure, resolubilized in water and finally, lyophilized. Then, peptides were dissolved in solvent A and purified by semi-preparative HPLC using solvent A (95% water, 5% acetonitrile, 0.1% trifluoroacetic acid) and solvent B (100% acetonitrile, 0.1% trifluoroacetic acid) with a 10 min isocratic elution (100% A) followed by a 45 min linear gradient (up to 95% B) with a UV detection at 214 nm. The resulting solutions were evaporated under reduced-pressure and double-lyophilized. Purity of each peptide was evaluated by analytical reversed-phase HPLC using solvent A′ (95% water, 5% acetonitrile, 0.1% formic acid) and solvent B′ (100% acetonitrile, 0.1% formic acid) with a 5 min isocratic elution (100% A′) followed by a 25 min linear gradient (0% to 40% solvent B′) and a 10 min linear gradient (40% to 100% B′) with a UV detection at 214 nm. All the chemical characterizations (NMR, HRMS and HPLC) are provided in ESI.†

Potentiometric measurements

The pH-potentiometric titrations were investigated in the pH range 2.0–11.2 and 2.0–7.5 for the ligands and iron(III)-containing systems, respectively (I = 0.1 M $NaNO_3$ and T = 298.0 ± 0.1 K). A Dosimat 715 (Metrohm) automatic burette and pH-meter equipped with a semi-micro combined electrode (Metrohm) was used for the titration. The initial concentration of peptides was 2×10^{-3} M, using 1 : 1 and 1 : 2 metal-to-ligand ratios. The titrations were performed with carbonate free stock solution of sodium hydroxide at known concentration. During the titration argon was bubbled through the samples to ensure the absence of oxygen and carbon dioxide. The recorded pH readings were converted to hydrogen ion concentration as described by Irving *et al.*[70] Protonation constants of the ligands and the overall stability constants ($\log \beta_{pqr}$) of the complexes were calculated from at least 3 independent titrations (*ca.* 70 data points per titration) by means of the general computational programs, PSEQUAD[71] and SUPERQUAD[72] using eqn (1) and (2).

$$pM + qH + rL \rightleftharpoons M_pH_qL_r \quad (1)$$

$$\beta_{pqr} = \frac{[M_pL_qH_r]}{[M]^p \cdot [L]^q \cdot [H]^r} \quad (2)$$

Antioxidant assays

MES (50 mM, pH 6.0) and HEPES (50 mM, pH 7.4) buffers were treated on Chelex100 to remove trace metal contaminants from the solution and prevent unwanted reactions before the different tests. In Amplex Red and 3-CCA tests, the buffers were replaced with water to determine the buffer effect on these reactions. Indeed, some organic buffer (HEPES, TRIS) show efficient radical scavenging activity preventing a correct measurement of H_2O_2 and $HO^\bullet$ radicals.[73] Thus, high-purity water treated on Chelex100 was used and the pH was adjusted by addition of 0.1 M NaOH. The stock solution at 2 mM of iron(III)–nitrate was prepared from analytical grade reagent in an acidic media (0.1 M HNO_3) to keep iron(III) ion in solution, its exact concentration was checked spectrophotometrically using complexometric titration. Peptides (FD_3K and FE_3K), EDTA and DFO ligand stock solutions at 2 mM were prepared using MES or HEPES buffer depending on the pH applied. To perform the tests, a semi-micro quartz cell with 1 cm optical pathway was used, the sample holder in the spectrophotometer was thermostated at 25 °C by a Peltier temperature controller. Note: NBT (for nitroblue tetrazolium) assays were performed to measure the superoxide anion radical formation; however, despites our many efforts no convincing conditions can be found because of interfering side effects (see ESI† for a deeper discussion) and the NBT assay was therefore discarded.

Ascorbate tests

For a standard assay, a 5 mM ascorbate stock solution was freshly prepared using MES or HEPES buffer depending on the pH applied. The absorbance of ascorbate was followed over 10 min at 265 nm (ε = 14 500 M^{-1} cm^{-1}), and at least 3 independent measurements were carried out. In a total volume of 1 mL, the final concentration of the components was 100 μM with 1 : 1 : 1 $AscH^-$: ligand : Fe(III) ratio. The pH was checked at the end of each assay. The reaction was triggered by the addition of ascorbate. As reference reaction, $AscH^-$ oxidation by ligands alone was also studied. The initial ascorbate oxidation rate was calculated from the slope of $[AscH^-] = f(t)$.

Amplex red assay

For this assay, all components except the iron(III) ion and Amplex Red reagent, were dissolved in 50 mM MES or 50 mM HEPES buffers or in Milli-Q water. The Amplex Red reagent was dissolved in DMSO : buffer mixture at 1 : 4 ratio. When the buffers were replaced with water to determine the buffer effect on this reaction, high-purity water was used and the pH was adjusted by addition of 0.1 M NaOH. The H_2O_2 production was detected by Amplex Red reagent in the presence of horseradish peroxidase (HRP, Scheme S2, ESI†) forming the compound Resorufin with λ_{abs} = 570 nm.[74] A working solution was first prepared containing 0.8 U mL^{-1} HRP and 200 μM Amplex Red reagent in a light-protected tube. 50 μL of this solution was placed in the total volume of 1 mL reaction mixture. The final concentration of the $AscH^-$ was 200 μM, and the ligand (peptides, EDTA or DFO) : Fe(III) : $AscH^-$ ratio was 1 : 1 : 4. The $AscH^-$ was the last reagent added thus initiating the reaction between O_2 and Fe(III), the pH was checked at the end of each reaction. A negative control containing only the working solution in buffer was necessary in order to monitor the background absorbance of the Amplex Red itself. The Resorufin formation was monitored by visible absorption spectroscopy at

570 nm at RT over 45 min (Fig. S9, ESI†). To determine the H_2O_2 concentration, a standard calibration curve was used. To obtain this calibration curve, a 20 mM hydrogen peroxide solution was previously titrated by permanganometry and then diluted successively.

Coumarin-3-carboxyilic acid (3-CCA) assay

The MES and HEPES buffers disturbed the fluorescent spectra and also had efficient $HO^{\bullet}$ radical scavenging activity, thus pure water treated on Chelex100 was used as a solvent and the pH was adjusted by adding 0.1 M NaOH. Thus, all the reagents were dissolved in Milli-Q water except of the 3-CCA, since it was only soluble in phosphate buffer (50 mM, pH 6.0 and pH 7.4). The concentration of 3-CCA stock solution was 5 mM. In the total volume of 2 mL, the final concentrations of the ascorbate and 3-CCA were both 125 μM, and the ratio of the reaction mixture was ligand (peptides, EDTA or DFO) : Fe(III) : $AscH^-$ = 1 : 1 : 2.5. The pH was checked at the end of the measurement. In the case of EDTA, the amount of all components was 10 times less than that of the other ligand systems. For the greater reproducibility of the measured data, each measurement was started by monitoring a blank sample (without any ascorbate) for 5 min, then the ascorbate was added to the sample. The reaction between 3-CCA and hydroxyl radical generating the fluorescent compound 7-OH-CCA was followed over 30 min at 25 °C at λ_{em} = 450 nm (λ_{ex} = 395 nm) by spectrofluorometry (Scheme S3 and Fig. S10, ESI†). The $HO^{\bullet}$ concentration was determined in different systems (at pH 6 and 7.4 with different ligands) by a standard calibration curve using commercially available 7-OH-CCA.

HRMS and HRMS/MS measurements

In order to investigate FD_3K ligand oxidation by $HO^{\bullet}$ radical, the following reaction mixtures were prepared at room temperature and analysed after 18 h by HRMS and HRMS/MS measurements: in a total volume of 1 mL at pH 6.0 in water (pH was adjusted by 0.1 M NaOH), the concentrations of FD_3K, Fe(III), 3-CCA, $AscH^-$ and H_2O_2 were all adjusted equal to 1 mM.

Conflicts of interest

There are no conflicts to declare.

Acknowledgements

The authors thank the ''Impact Biomolecules'' project of the ''Lorraine Université d'Excellence'' (Investissements d'avenir – ANR-15-IDEX-04-LUE) for financial support. The authors thanks L. Saidi for preliminary works, P. Lemiere, S. Parant and M. Achard for technical help.

Notes and references

1 R. Crichton, in *Biological Inorganic Chemistry*, ed. R. Crichton, Academic Press, 3rd edn, 2019, ch. 1, pp. 1–18.
2 S. V. Torti and F. M. Torti, *Nat. Rev. Cancer*, 2013, **13**, 342–355.
3 C. R. Ferreira and W. A. Gahl, *Transl. Sci. Rare Dis.*, 2017, **2**, 101–139.
4 F. Collin, *Int. J. Mol. Sci.*, 2019, **20**, 2407.
5 B. Halliwell, *J. Neurochem.*, 2006, **97**, 1634–1658.
6 K. M. Holmström and T. Finkel, *Nat. Rev. Mol. Cell Biol.*, 2014, **15**, 411–421.
7 M. Schieber and N. S. Chandel, *Curr. Biol.*, 2014, **24**, R453.
8 K. Jomova and M. Valko, *Toxicology*, 2011, **283**, 65–87.
9 Z. Liu, Z. Ren, J. Zhang, C.-C. Chuang, E. Kandaswamy, T. Zhou and L. Zuo, *Front. Physiol.*, 2018, **9**, 477.
10 A. M. Pisoschi and A. Pop, *Eur. J. Med. Chem.*, 2015, **97**, 55–74.
11 M. Wojcik, I. Burzynska-Pedziwiatr and L. Wozniak, *Curr. Med. Chem.*, 2010, **17**, 3262–3288.
12 J. L. Lau and M. K. Dunn, *Bioorgan. Med. Chem.*, 2018, **26**, 2700–2707.
13 K. Fosgerau and T. Hoffmann, *Drug Discovery Today*, 2015, **20**, 122–128.
14 N. J. Kang, H.-S. Jin, S.-E. Lee, H. J. Kim, H. Koh and D.-W. Lee, *Crit. Rev. Environ. Sci. Technol.*, 2020, **50**, 72–103.
15 B. H. Sarmadi and A. Ismail, *Peptides*, 2010, **31**, 1949–1956.
16 R. Esfandi, M. E. Walters and A. Tsopmo, *Heliyon*, 2019, **5**, e01538.
17 L. L. S. Canabady-Rochelle, K. Selmeczi, S. Collin, A. Pasc, L. Muhr and S. Boschi-Muller, *Food Chem.*, 2018, **239**, 478–485.
18 J. Bechaux, P. Gatellier, J.-F. Le Page, Y. Drillet and V. Sante-Lhoutellier, *Food Funct.*, 2019, **10**, 6244–6266.
19 E. C. Y. Li-Chan, *Curr. Opin. Food Sci.*, 2015, **1**, 28–37.
20 A. Carocci, A. Catalano, M. S. Sinicropi and G. Genchi, *Biometals*, 2018, **31**, 715–735.
21 P. Poprac, K. Jomova, M. Simunkova, V. Kollar, C. J. Rhodes and M. Valko, *Trends Pharmacol. Sci.*, 2017, **38**, 592–607.
22 D. Denoyer, S. Masaldan, S. La Fontaine and M. A. Cater, *Metallomics*, 2015, **7**, 1459–1476.
23 N. R. Perron and J. L. Brumaghim, *Cell Biochem. Biophys.*, 2009, **53**, 75–100.
24 M. Samsonowicz, E. Regulska and M. Kalinowska, *Chem. – Biol. Interact.*, 2017, **273**, 245–256.
25 M. M. Kasprzak, A. Erxleben and J. Ochocki, *RSC Adv.*, 2015, **5**, 45853–45877.
26 D. Xu, M.-J. Hu, Y. Q. Wang and Y. L. Cui, *Molecules*, 2019, **24**, 1123.
27 M. B. H. Youdim, *Exp. Neurobiol.*, 2010, **19**, 1–14.
28 L. Belguendouz, L. Fremont and A. Linard, *Biochem. Pharmacol.*, 1997, **53**, 1347–1355.
29 A. Shakeri, Y. Panahi, T. P. Johnston and A. Sahebkar, *BioFactors*, 2019, **45**, 304–317.
30 J. M. Lü, P. H. Lin, Q. Yao and C. Chen, *J. Cell. Mol. Med.*, 2010, **14**, 840–860.
31 H. Zheng, L. M. Weiner, O. Bar-Am, S. Epsztejn, Z. I. Cabantchik, A. Warshawsky, M. B. H. Youdim and M. Fridkin, *Bioorg. Med. Chem.*, 2005, **13**, 773–783.
32 R. C. Hider, S. Roy, Y. M. Ma, X. Le Kong and J. Preston, *Metallomics*, 2011, **3**, 239–249.

33 E. Farkas and I. Sóvágó, in *Amino Acids, Peptides and Proteins*, The Royal Society of Chemistry, 2017, vol. 41, pp. 100–151.
34 I. Sóvágó, K. Várnagy, N. Lihi and Á. Grenács, *Coord. Chem. Rev.*, 2016, **327–328**, 43–54.
35 N. Lihi, M. Lukács, M. Raics, G. Szunyog, K. Várnagy and C. Kállay, *Inorgan. Chim. Acta*, 2018, **472**, 165–173.
36 L. R. Perez and K. J. Franz, *Dalton Trans.*, 2010, **39**, 2177–2187.
37 T. Zheng and E. M. Nolan, *Metallomics*, 2012, **4**, 866–880.
38 C. Kurth, H. Kage and M. Nett, *Org. Biomol. Chem.*, 2016, **14**, 8212–8227.
39 R. C. Hider and X. Kong, *Nat. Prod. Rep.*, 2010, **27**, 637–657.
40 R. D. Hancock and A. E. Martell, *Chem. Rev.*, 1989, **89**, 1875–1914.
41 A. Galano and A. Cruz-Torres, *Org. Biomol. Chem.*, 2008, **6**, 732–738.
42 B. R. Ipson and A. L. Fisher, *Ageing Res. Rev.*, 2016, **27**, 93–107.
43 C. A. Damante, K. Ősz, Z. Nagy, G. Pappalardo, G. Grasso, G. Impellizzeri, E. Rizzarelli and I. Sóvágó, *Inorg. Chem.*, 2008, **47**, 9669–9683.
44 R. L. Thurlkill, G. R. Grimsley, J. M. Scholtz and C. N. Pace, *Protein Sci.*, 2006, **15**, 1214–1218.
45 E. Farkas, É. A. Enyedy and H. Csóka, *Polyhedron*, 1999, **18**, 2391–2398.
46 A. E. Martell, R. M. Smith, A. E. Martell and R. M. Smith, in *Critical Stability Constants*, ed. A. E. Martell and R. M. Smith, Springer, 1982.
47 A. Stefánsson, *Environ. Sci. Technol.*, 2007, **41**, 6117–6123.
48 B. K. Fuqua, C. D. Vulpe and G. J. Anderson, *J. Trace Elem. Med. Biol.*, 2012, **26**, 115–119.
49 S. Gulec, G. J. Anderson and J. F. Collins, *Am. J. Physiol.: Gastrointest. Liver Physiol.*, 2014, **307**, G397–G409.
50 H. Lv and P. Shang, *Metallomics*, 2018, **10**, 899–916.
51 T. Kurz, J. W. Eaton and U. T. Brunk, *Int. J. Biochem. Cell Biol.*, 2011, **43**, 1686–1697.
52 R. B. Martin, J. Savory, S. Brown, R. L. Bertholf and M. R. Wills, *Clin. Chem.*, 1987, **33**, 405–407.
53 Y. Kohgo, K. Ikuta, T. Ohtake, Y. Torimoto and J. Kato, *Int. J. Hematol.*, 2008, **88**, 7–15.
54 Z. I. Cabantchik, *Front. Pharmacol.*, 2014, **5**, 45.
55 H. Drechsel and G. Jung, *J. Pept. Sci.*, 1998, **4**, 147–181.
56 I. Bertini, C. Luchinat, G. Parigi and E. Ravera, in *NMR of Paramagnetic Molecules*, ed. I. Bertini, C. Luchinat, G. Parigi and E. Ravera, Elsevier, 2nd edn, 2017, ch. 7, pp. 175–253.
57 S. Balayssac, I. Bertini, C. Luchinat, G. Parigi and M. Piccioli, *J. Am. Chem. Soc.*, 2006, **128**, 15042–15043.
58 L. T. Dalvi, D. C. Moreira, R. Andrade, J. Ginani, A. Alonso and M. Hermes-Lima, *Spectrochim. Acta, Part A*, 2017, **173**, 910–917.
59 V. A. Roginsky, T. K. Barsukova, G. Bruchelt and H. B. Stegmann, *Biochim. Biophys. Acta, Gen. Subj.*, 1997, **1335**, 33–39.
60 R. T. Dean and P. Nicholson, *Free Radical Res.*, 1994, **20**, 83–101.
61 S. Singh and R. C. Hider, *Anal. Biochem.*, 1988, **171**, 47–54.
62 P. Holden and L. S. Nair, *Tissue Eng., Part B*, 2019, **25**, 461–470.
63 E. Atrián-Blasco, M. Del Barrio, P. Faller and C. Hureau, *Anal. Chem.*, 2018, **90**, 5909–5915.
64 R. R. Grinstead, *J. Am. Chem. Soc.*, 1960, **82**, 3464–3471.
65 W. G. Gutheil, M. E. Stefanova and R. A. Nicholas, *Anal. Biochem.*, 2000, **287**, 196–202.
66 T. Brumbarova, C. Le and P. Bauer, *Bio-Protoc.*, 2016, **6**, e1999.
67 Y. Manevich, K. D. Held and J. E. Biaglow, *Radiat. Res.*, 1997, **148**, 580–591.
68 X. Solans, M. Font Altaba and J. Garcia-Oricain, *Acta Crystallogr., Sect. C: Cryst. Struct. Commun.*, 1984, **40**, 635–638.
69 J. L. Hougland, J. Darling and S. Flynn, in *Molecular Basis of Oxidative Stress, Chemistry, Mechanics and Disease Pathogenesis*, ed. F. A. Villamena, 1st edn, 2013, ch. 3, pp. 71–92.
70 H. M. Irving, M. G. Miles and L. D. Pettit, *Anal. Chim. Acta*, 1967, **38**, 475–488.
71 L. Zekany and I. Nagypal, in *Computational Methods for the Determination of Formation Constants*, ed. D. J. Leggett, Springer, 1985, ch. 8, pp. 291–353.
72 P. Gans, A. Sabatini and A. Vacca, *J. Chem. Soc., Dalton Trans.*, 1985, 1195–1200.
73 M. Hicks and J. M. Gebicki, *FEBS Lett.*, 1986, **199**, 92–94.
74 M. Zhou, Z. Diwu, N. Panchuk-Voloshina and R. P. Haugland, *Anal. Biochem.*, 1997, **253**, 162–168.